

Cosmological parameters from VSA, CBI and other data: a Monte-Carlo approach

Antony Lewis^{1,*} and Sarah Bridle^{2,†}

¹*DAMTP, CMS, Wilberforce Road, Cambridge CB3 0WA, UK.*

²*Institute of Astronomy, Madingley Road, Cambridge, CB3 0HA, UK.*

We present a fast Markov Chain Monte-Carlo exploration of cosmological parameter space. We perform a joint analysis of results from the recent CMB experiments, including CBI and VSA, and provide a practical set of parameter constraints from the CMB independent of other data. We next combine CMB, HST Key Project, large scale structure, supernovae and nucleosynthesis data. The Monte Carlo method allows us to rapidly investigate a large number of parameters, and we present results from an 11 cosmological parameter analysis, as well as results from a better constrained 9 parameter analysis motivated by inflationary models. In a series of appendices we describe the publically available code, explain the use of importance sampling for quickly computing results from new data and discuss the different ways of converting parameter samples to parameter constraints. We also assess the goodness of fit and consistency, and describe the use of analytic marginalization over normalization parameters.

I. INTRODUCTION

There is now a wealth of data from cosmic microwave background (CMB) observations and growing amount of information on large scale structure from a wide range of sources. We would like to extract the maximum amount of information from this data, usually conveniently summarized by estimates of a set of cosmological parameter values. With high quality data one can constrain a large number of parameters, which in principle allows us not only to put estimates and error bars on various quantitative parameters, but also to address more fundamental qualitative questions: Do we observe primordial gravitational waves? Do the neutrinos have a cosmologically significant mass? Is the universe flat? Are the standard model parameters those that best account for the data? In addition the consistency of the different data sets with respect to a cosmological model can be assessed.

Recent work involving parameter estimation from the CMB includes Refs. [1], [2], [3], [4] [5], [6] and [7] In this paper we employ Markov Chain Monte Carlo (MCMC) techniques[8, 9, 10], as advocated for Bayesian CMB analysis in Ref. [11] and demonstrated by Ref. [3]. By generating a set of MCMC chains we can obtain a set of independent samples from the posterior distribution of the parameters given the data. From a relatively small number of these samples one can estimate the marginalized posterior distributions of the parameters, as well as various other statistical quantities. The great advantage of the MCMC method is that it scales, at its best, approximately linearly with the number of parameters, allowing us to include many parameters for only small additional computational cost. The samples also probe the shape of the full posterior, giving far more information than just the marginalized distributions.

In section II we present constraints from the latest CMB data, illustrating the MCMC method. We defer a brief introduction to the MCMC method and a description of our implementation and terminology to Appendix A. The method of importance sampling is also illustrated in section II, and is described in detail Appendix B, where we explain how it can be used to take into account different priors on the parameters, new data, and for accurate but fast estimation given a good approximation to the theoretical model predictions. We add large scale structure, supernova and cluster normalisation information in section III so that more parameters can be constrained. We compare flat models with ‘inflationary’ priors (9 cosmological parameters) and then a more general model (11 cosmological parameters). For this paper we compute all theoretical (CMB and matter power spectrum) predictions numerically using the fast Boltzmann code CAMB [12] (a parallelized version of CMBFAST [13]), and therefore our results are accurate and could be generalized very easily to include any additional parameters that can be accounted for by small modifications of a Boltzmann code.

*Electronic address: Antony@AntonyLewis.com

†Electronic address: sarah@ast.cam.ac.uk

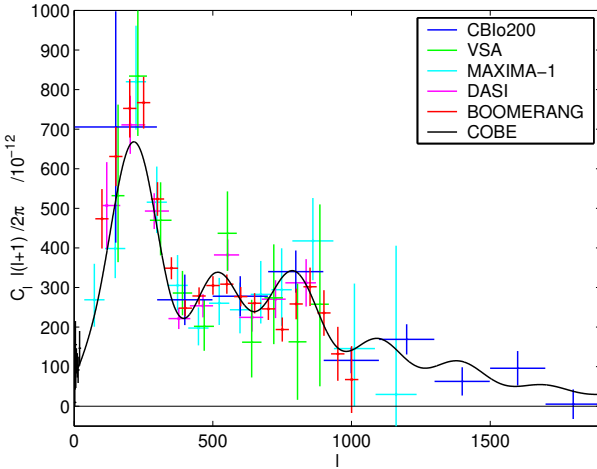


FIG. 1: The CMB data used in this paper. Note that we use only CBI data with $\ell < 2000$ so as not to risk influence by any secondary anisotropies that might produce non-negligible power on smaller scales.

II. CMB CONSTRAINTS

We use the results of the COBE [14], BOOMERANG [5], MAXIMA [15], DASI [16], VSA [17] and CBI [18] observations in the form of band power estimates for the temperature CMB power spectrum. These data are plotted in Fig. II. The very small angular scale results from CBI have been discussed extensively in [18, 19] and do not fit the linear predictions of standard acoustic oscillation models. Therefore for the purposes of this paper we assume that the small scale power observed by CBI has its origin in non-linear or non-standard small scale effects that we do not attempt to model, and so use only the mosaic (rather than deep pointing) data points throughout. In addition we use only the first 9 points ($\ell < 2000$) from the odd binning of the mosaic fields since above that the noise in the bandpowers becomes much larger than the prediction for the class of models we consider.

For COBE we use the offset-lognormal band-powers and covariance matrix from RADPACK [20]. For DASI and VSA we also use the offset-lognormal bandpowers and integrate numerically over an assumed Gaussian calibration uncertainty. For BOOMERANG, MAXIMA and CBI we assume that the band-power likelihood distributions are Gaussian, and marginalize analytically over the calibration and beam uncertainties (where appropriate) assuming they are also Gaussian [21]. We also assume top hat window functions for these data, and neglect correlations between data points. Using the sets of samples obtained it is a simple matter to account for small corrections when the required information is publicly available (see Appendix B).

The base set of cosmological parameters we sample over are $\omega_b = \Omega_b h^2$ and $\omega_c \equiv \Omega_c h^2$, the physical baryon and CDM densities relative to the critical density, Ω_Λ , the ratio of the critical density in the form of dark energy, $\Omega_K \equiv 1 - \Omega_{\text{tot}}$ measuring the spatial curvature, z_{re} , the redshift at which the reionization fraction is a half, and A_s , measuring the initial power spectrum amplitude. Throughout we use at least the priors that $4 < z_{\text{re}} < 20$, $0.4 < h < 1.0$, $-0.3 < \Omega_K < 0.3$, $\Omega_\Lambda > 0$, and that the age of the universe, t_0 , is $10 \text{ Gyr} < t_0 < 20 \text{ Gyr}$. The significance of this base set is that this defines the Bayesian priors: there is a flat prior on each parameter of the base set. We discuss later how we assess the significance of these priors, and highlight our main results, which are largely independent of the priors. The above additional constraints on h , Ω_Λ , Ω_K and the age have little effect on the joint results since the cut-off values are well into the tails of the distribution. However for the purpose of the Monte-Carlo it is very convenient to be able to quickly reject models in the extreme tails without having to compute the theoretical predictions. Throughout we assume purely adiabatic primordial perturbations, though our approach could easily be generalized to include isocurvature modes.

MCMC illustration

An MCMC sampler can be thought of as a black box whose input is a function for calculating the probability given a list of parameter values, and whose output is a list of samples. A single sample is a coordinate in the n-d parameter space, and the sampling method ensures that the number density of samples is asymptotically proportional to the probability density. As an illustration, in the left hand panel of Figure 2 we show the values of the total matter

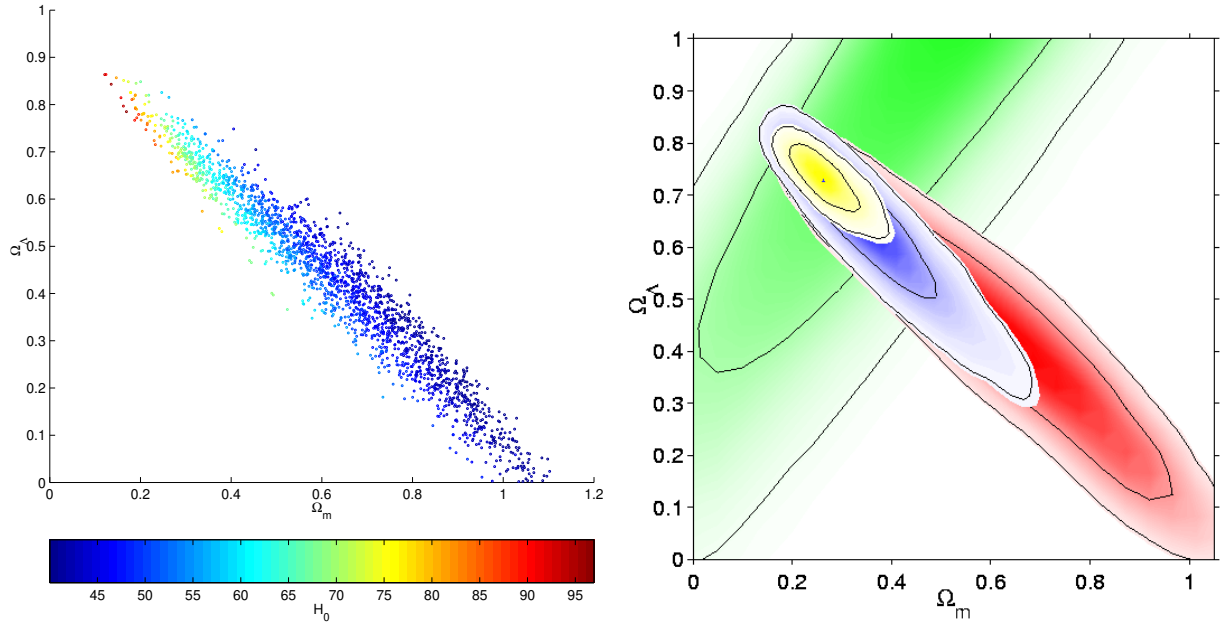


FIG. 2: *Left:* 2000 samples from the posterior distribution of the parameters plotted by their Ω_m and Ω_Λ values. Points are colored according to the value of H_0 of each sample. We assume the base parameter set with broad top-hat priors. *Right:* bottom layer (green): supernova constraints; next layer up (red): CMB data alone; next (blue): CMB data plus HST Key Project prior; top layer (yellow): all data combined (see text). 68 and 95 per cent confidence limits are shown.

density, $\Omega_m = \Omega_b + \Omega_c$, and cosmological constant, Ω_Λ , for samples collected from an MCMC run using the CMB data and base parameters discussed in the previous paragraphs.

Note that although Ω_m is not one of our base set of parameters, it is simple to find probabilities as a function of Ω_m by taking the parameter values in each sample and deriving the corresponding values of Ω_m . Since the MCMC method produces samples from the full posterior, it follows that the number density of samples in this two-dimensional plane is proportional to the probability density of the two parameters, marginalised over all the other parameters. Note that this refers to the fully marginalised probability density rather than any conditional or projected probability density. The familiar direction of CMB degeneracy along the flat universe line is apparent. The colors of the dots indicate the Hubble constant value for each sample, as given in the color bar. This shows that the high Ω_m tail of samples are due entirely to low H_0 regions of parameter space, illustrating the point made in e.g. [22] that a Hubble constant prior alone combined with the CMB can put useful limits on Ω_m and Ω_Λ without the need for supernova constraints.

The likelihood as a function of position in the Ω_m - Ω_Λ plane from CMB data alone is shown by the red contours in the right hand panel of Figure 2. Note that compared to other CMB only plots the contours close slightly at high Ω_m , which is due to our lower limit on the Hubble constant of $h > 0.4$. The 2-d likelihoods shown are calculated from the samples by estimating the probability density at a grid of points using a Gaussian weighting kernel and then using interpolation to draw the contour lines. This produces a plot very similar to that obtained using a grid integration calculation of the marginalized posterior (assuming there are no small scale features in the posterior).

Extra data can be taken into account quickly by re-weighting the samples, a technique known as *importance sampling* (described in detail in Appendix B). The posterior is simply re-calculated at each sample position, and a weight assigned to the sample according to the ratio of the new posterior to the old posterior. For example, using a Gaussian HST Key Project [23] prior on the Hubble constant $H_0 = 72 \pm 8 \text{ km s}^{-1}\text{Mpc}^{-1}$ we obtain the blue contours plotted in the right hand panel of Figure 2.

Using importance sampling we have checked that the CMB datasets are consistent using the hyperparameter method, as described in Appendix E.

Parameter	pre VSA/CBI	+VSA+CBI
$\Omega_b h^2$	0.0213 ± 0.0021	0.0210 ± 0.0021
n_s	0.975 ± 0.046	0.963 ± 0.045
$\sigma_8 \exp(0.04 - \tau)(h/0.7)^{-2.7}(\Omega_m/0.3)^{-1.1}$	0.854 ± 0.038	0.841 ± 0.037
$\sigma_8 \exp(0.04 - \tau)(h/0.7)^{0.39}(\Omega_m/0.3)^{-0.049}$	0.757 ± 0.063	0.745 ± 0.059

TABLE I: Marginalised parameter constraints (68 per cent confidence) from two combinations CMB data alone assuming a flat universe and the base parameter set described in the text. Extra digits are inserted to help comparison between pre and post VSA and CBI.

Quantitative constraints from CMB data alone

Above we illustrated the MCMC method in the Ω_m - Ω_Λ plane for a 7 parameter cosmological model. Clearly not all of the possible cosmological parameters can be constrained by the current CMB data alone. Fortunately some reasonable, although fairly conservative, theoretical prejudices can be used to limit the parameter space to 6 parameters, and we present the results of such an analysis here. We fix $\Omega_K = 0$, therefore the parameters varied are ω_b , ω_c , n_s , Ω_Λ , z_{re} , A_s (as described above). The only parameters that can be reasonably disentangled are Ω_b and n_s , from the 2nd and 3rd acoustic peak heights respectively. These constraints are given in the right hand column of Table I and are in accordance with previous similar analyses and BBN. In addition there will be constraints on 3 orthogonal combinations of the remaining parameters, e.g. parameterised by σ_8 , Ω_m , h and τ (where τ is the optical depth to reionisation, which can be calculated from z_{re} as detailed in e.g. [24].) Since $\Omega_b h^2$ and n are not too correlated with the other parameters, we marginalise over them and look in the remaining four dimensional parameter space. By freezing τ at a range of values and looking at eigenvectors in the logs of σ_8 , Ω_m , h we find that the two combinations given in Table I are constrained relatively independently of any other parameter, although the errors are too large on any third constraint to be worth quoting. Thus although much information is lost on attempting to obtain constraints on the individual cosmological parameters, the above can still be used, e.g. in a simple χ^2 to encapsulate the CMB constraints (bearing in mind the theoretical assumptions used).

While restricted to this relatively small parameter space we take this opportunity to investigate the relative impacts of the new VSA and CBI results. We note that using a smaller parameter space will, if anything, tend to emphasize the effects of the new results, relative to if a larger parameter space were investigated. This is because the error bars on each parameter always effectively have a contribution from the random experimental errors and also due to parameter degeneracies. These parameter degeneracies are reduced on using a smaller parameter set. We redo the above 6 parameter analysis using only the pre VSA/CBI data, and the results are shown in the left hand column of Table I. For simplicity we assume use the same power law approximation for the combination of σ_8 , h , Ω_m and τ as derived above. The peaks move by a fraction of the error, and the error bars are fractionally smaller.

III. ADDITIONAL COSMOLOGICAL CONSTRAINTS

The CMB data alone can only provide a limited number of constraints so before extending the parameter space to make full use of the Monte-Carlo method it is useful to include as much relatively reliable data as possible. Some published parameter constraints assume particular values for parameters that we wish to vary. As a simple example, the Supernova Cosmology Project has made available constraints in Ω_m - Ω_Λ space, which could only be used if the quintessence parameter $w = -1$ were assumed, and one assumes the same priors. Fortunately the full supernova data are available, which we use (described below). However this is not always practical, for example in the case of σ_8 - Ω_m estimates from cluster number counts or cosmic shear. In these cases we increase the error bars to encompass systematic effects due to other parameters, which ensures that the resulting MCMC chains will cover all of the relevant parameter space, and can then be importance sampled later with a tighter constraint. If the chains are generated too tightly constrained one cannot recover information about the excluded parameter space.

Nucleosynthesis constraints suggest $\omega_b \approx 0.02$ [25], and we assume the Gaussian prior $\omega_b = 0.02 \pm 0.002$, (1σ) which is somewhat broader than the error quoted in Ref. [25] to allow for differences with other estimations. We include Type 1A supernovae data from [26], using the effective magnitudes and errors from the 54 supernovae that they included in the primary fit (fit C). We marginalize analytically with a flat prior on the intrinsic magnitudes, which is equivalent (within an irrelevant multiplicative constant) to evaluating the likelihood at the best fit value (see Appendix F). We neglect the small correlations but multiply the log likelihood by 50/54 to account for the effective degrees of freedom quoted in Ref [26]. There is currently controversy about the value of σ_8 , with different authors giving a range of results. We use $\sigma_8(\Omega_m/0.3)^{0.44} = 0.7 \pm 0.15$ as a crude encapsulation of these, to including

the systematic variations.¹ We use the galaxy power spectrum from the first 100,000 redshifts of the 2dF galaxy redshift survey ([29]). We assume that this is directly proportional to the matter power spectrum at $z = 0$, in other words that the bias and evolution are scale independent. We assume a flat prior on the proportionality constant and marginalize analytically as described in Appendix F.

We now demonstrate the power of the Monte-Carlo method by using the above data to constrain a larger number of parameters. We generate the theoretical matter power spectrum, σ_8 , and CMB power spectra for each model using CAMB, using the proposal density described in Appendix A to exploit the differing computational costs of changing the various parameters. We consider separately the case of inflationary models, which are flat, and more general models less constrained by theoretical prejudice. In both cases we include f_ν , the fraction of the dark matter that is in the form of massive neutrinos², and allow for an effective constant equation of state parameter³ $w \equiv p/\rho$ for the homogeneous dark energy, and assume that $-1 \leq w < 0$.

Inflationary models

The simplest single-field inflationary models predict a flat universe and can be described quite accurately by the slow-roll approximation. The shape and amplitude of the initial curvature perturbation depends on the shape of the inflationary potential, often encoded in ‘slow-roll parameters’ which are assumed to be small, plus an overall normalization which depends on the Hubble rate when the modes left the horizon during inflation. The initial curvature perturbation and tensor power spectra are usually parameterized as

$$P_\chi(k) = A_s \left(\frac{k}{k_{s0}} \right)^{n_s-1} \quad P_h(k) = A_t \left(\frac{k}{k_{t0}} \right)^{n_t}$$

where n_s and n_t are the conventional definitions of the scalar and tensor spectral indices. At the lowest order approximation, the slow-roll initial power spectrum is determined from the inflationary potential V by the slow-roll parameter parameters ϵ_1, ϵ_2 by [33]

$$\epsilon_1 = 16A_t/A_s = \frac{m_{\text{Pl}}^2}{16\pi} \left(\frac{V'}{V} \right)^2 \quad (1)$$

$$n_s = 1 - 2\epsilon_1 - \epsilon_2 \equiv 1 - \frac{m_{\text{Pl}}^2}{8\pi} \left[3 \left(\frac{V'}{V} \right)^2 - \frac{V''}{V} \right] \quad (2)$$

$$A_s = \frac{H^2}{\pi\epsilon_1 m_{\text{Pl}}^2} \quad (3)$$

where quantities are evaluated when $Ha = k_*$ (we use $k_* = k_{s0} = k_{t0} = 0.01 \text{Mpc}^{-1}$). Using the above parameters is thus equivalent to using the free parameters $A_s, A_t/A_s, n_s$ that one would use in more general models, plus the inflationary constraint that the spectral index of the tensor modes is given by $n_t = -2\epsilon_1$. From the definition it is clear that $\epsilon_1 \geq 0$, and except in contrived models one also expects $n_s \leq 0$, though we do not enforce this. Simple ekpyrotic models are consistent with this parameterization when there are no tensor modes.

Figure 3 shows the fully marginalized posterior constraints on the various parameters using the CMB, 2dF, supernovae, HST, cluster and nucleosynthesis constraints, using 2500 weakly correlated samples. The results are Monte-Carlo marginalized over all 8 of the other parameters and also analytically or numerically marginalized over the calibration uncertainties, etc, as previously discussed. It is important to check that the parameters are really being constrained, in the sense that the results are relatively insensitive to the priors, so in addition to the marginalized posterior we also plot the mean likelihood of the samples. These will differ when the result is sensitive to the parameter space volume available, which can change as the result of choosing different priors (see Appendix C). In Figure 4 we show a sample of 2D plots, with confidence contours from the marginalized distribution, and shaded according to the

¹ We are not accounting for the high- l power in the CBI data, which could possibly indicate a much higher σ_8 value [19, 27], though there are other possibilities [28].

² We assume three neutrinos of degenerate mass, as indicated by the atmospheric and solar neutrino oscillation observations [30, 31], and compute the evolution using the fast but accurate method described in Ref. [32].

³ Quintessence does not predict a constant equation of state parameter, however for many quintessence models one would expect a better fit assuming $w \neq -1$ than fixing $w = -1$ (equivalent to a cosmological constant). Perturbations to the quintessence field have only a small effect on large scales where cosmic variance dominates anyway.

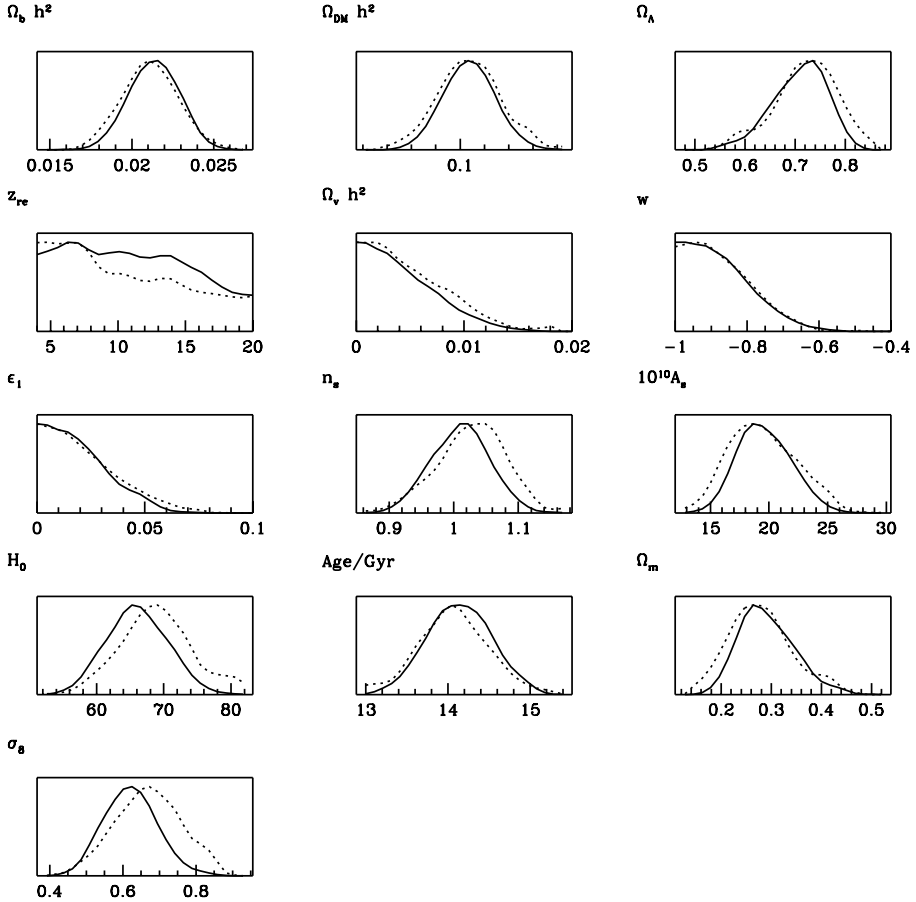


FIG. 3: Posterior constraints for flat inflationary models. The solid lines show the fully marginalized posterior, the dotted lines show the mean relative mean posterior of the samples. The curves are generated from the MCMC samples using a Gaussian smoothing kernel 1/20th the width of each plot.

mean likelihood of the samples. It is clear that we do have genuine constraints, though the marginalized value of the derived parameter H_0 is slightly biased towards low values by our choice of fundamental variables.⁴

As discussed in Appendix C, it can be useful to have parameter confidence limits from the full N -dimensional distribution, as well as limits from the one dimensional marginalized distribution. We show the marginalized and N -dimensional parameter constraints with the inflationary assumptions in Table II. Monte-Carlo samples from the posterior do not provide accurate estimates of the parameter best-fit values (in high dimensions the best-fit region is typically has a much higher likelihood than the mean, but it occupies a minuscule fraction of parameter space), nor of the high-significance limits do to the scarcity of samples in these regions.⁵

The combined datasets provide good constraints on the neutrino mass, despite the large parameter space. The limits given in Table II for $\Omega_\nu h^2$ translate into a limit on the neutrino mass via

$$\Omega_\nu h^2 = \frac{\sum m_\nu}{93.8 \text{ eV}} \quad \Rightarrow \quad m_\nu \approx 31 \Omega_\nu h^2 \text{ eV},$$

⁴ There are more ways to choose Ω_b and Ω_c and Ω_Λ to get a flat universe compatible with the data if H_0 is low, because the physics depends predominantly upon the physical matter densities $\Omega_b h^2$ and $\Omega_c h^2$.

⁵ If you wish to compute accurate estimates in the tails of the distribution the trick is to sample from a broader distribution and then importance sample to the correct distribution, for example by originally sampling from $P^{1/T}$ where $T > 1$.

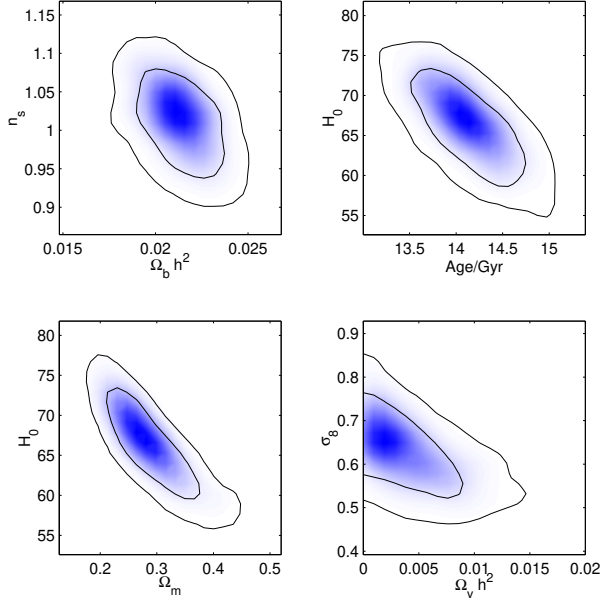


FIG. 4: Posterior constraints for flat inflationary models. The contours show the 68% and 95% confidence limits from the marginalized distribution. The shading shows the mean likelihood of the samples.

	Mean	Best-fit	68%-1D	95%-1D	68%-full	95%-full
$\Omega_b h^2$	0.022	0.021	0.020 – 0.0226	0.019 – 0.0235	0.017 – 0.025	0.016 – 0.026
$\Omega_{DM} h^2$	0.106	0.108	0.095 – 0.112	0.089 – 0.120	0.075 – 0.130	0.071 – 0.137
Ω_Λ	0.722	0.718	0.67 – 0.75	0.63 – 0.79	0.57 – 0.82	0.56 – 0.84
$\Omega_\nu h^2$	0.004	0.003	< 0.005	< 0.015	< 0.013	< 0.016
w	-0.89	-0.98	< -0.85	< -0.72	< -0.63	< -0.55
ϵ_1	0.02	0.014	< 0.023	< 0.05	< 0.07	< 0.08
n_s	1.03	1.03	0.98 – 1.05	0.95 – 1.08	0.90 – 1.15	0.88 – 1.15
σ_8	0.63	0.65	0.57 – 0.68	0.54 – 0.74	0.46 – 0.82	0.43 – 0.86
Age/Gyr	14.4	14.2	13.8 – 14.5	13.7 – 14.7	13.1 – 15.1	13.1 – 15.2
H_0	67	67	63 – 70	60 – 73	57 – 80	55 – 80

TABLE II: Parameter constraints for inflationary models. 1D limits are from the confidence interval of the fully marginalized 1D distribution, the full limits give the extremal values of the parameters in the full N -dimensional confidence region (see Appendix C for discussion). The best-fit and 95% values are unlikely to be accurate.

where the last equality follows from our assumption that there are three neutrinos of approximately degenerate mass, as indicated by the small mass-squared differences detected by the neutrino oscillation experiments [30, 31]. We therefore find the result $m_\nu \lesssim 0.5$ eV at 95% confidence, the marginalized and N -dimensional limits agreeing in this case (Monte-Carlo sampling noise on these estimates should be neither large nor negligible). These result account for the shape of the full inflationary parameter space posterior, and are consistent with the limits found in Refs. [34, 35] under more restricted assumptions. The simplest model where all the neutrino masses are very small is still a good bet.

The tensor amplitude (encoded here via ϵ_1) is degenerate with the reionization redshift since both change the relative CMB power on large and small scales. When tensors are included z_{re} becomes more of a nuisance parameter that can only be very weakly constrained; if the tensor contribution is unconstrained it can have a much larger effect than the reionization if we assume that $4 < z_{\text{re}} < 20$.

The method we have used could be generalized for a more accurate parameterization of the initial power spectrum, for example going to second order in the slow-roll parameters [33], which in general introduces a running in the spectral index. The current data is however clearly consistent with the simplest scale invariant power spectrum with no tensor modes.

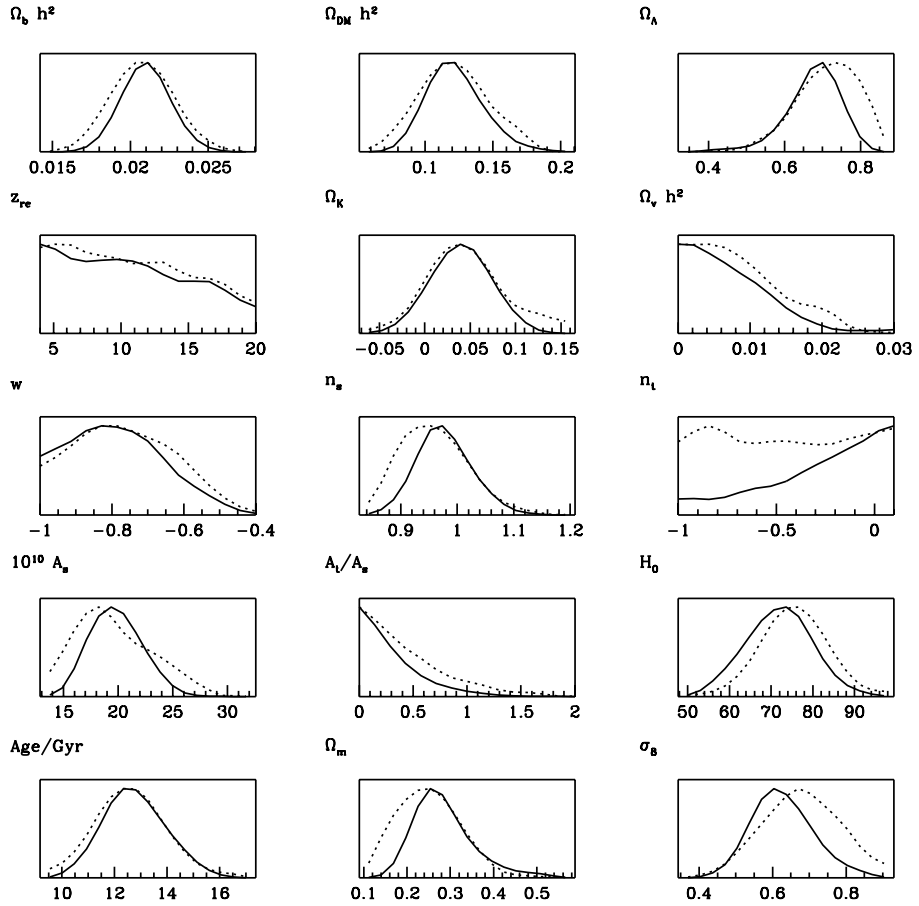


FIG. 5: Posterior constraints for general models. Some sampling noise is apparent, particularly on the dotted mean likelihood lines.

General models

We now relax the constraint on the curvature, and allow the tensor spectral index to be a free parameter (we assume $n_t \leq 0.1$). We parameterize the power spectra of the initial curvature and tensor metric perturbations as in the inflationary case⁶, except that we now report results for A_t/A_s rather than a slow-roll parameter, and choose the scalar and tensor pivot scales $k_{s0} = 0.05\text{Mpc}^{-1}$, $k_{t0} = 0.002\text{Mpc}^{-1}$.

In Figure 5 we show the parameter constraints that we get using 2300 weakly correlated samples from the 11-parameter MCMC run. The tensor spectral index is essentially unconstrained, the difference between the mean likelihood and marginalized 1D plots being due to the assumed flat prior on the tensor amplitude - at very small amplitudes clearly n_t could be anything and still be undetectable. In this analysis it seems that slightly open models are favoured, though as shown in Figure 6 a flat universe with $w = -1$ is within the 68% confidence contour (since we have relatively few samples the exact position of the contours in 2D should not be taken too seriously). The limits on w and the neutrino mass are rather broader than with inflationary assumptions, as one might expect given that the relaxation of the flatness assumption.

⁶ For non-flat models our definitions follow [36]. In open models we assume the tensor power spectrum has an additional factor of $\tanh(\pi\sqrt{-k^2/K - 3}/2)$ on the right hand side.

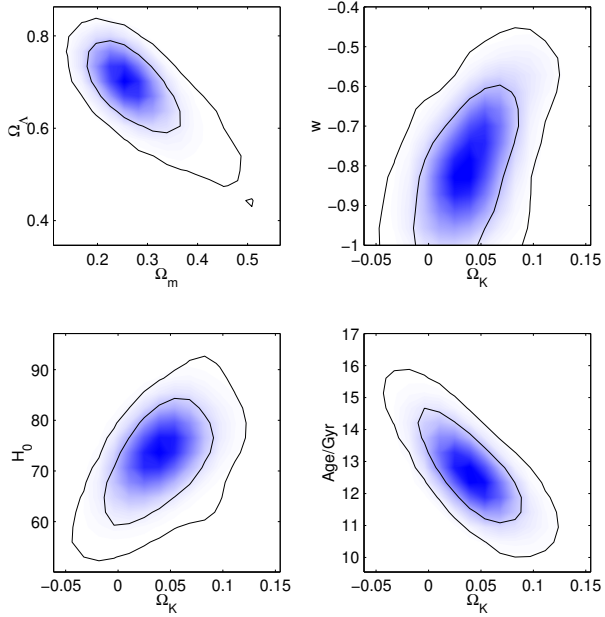


FIG. 6: Posterior constraints for general models.

Comparing the models

We have explored the posterior distribution in various parameter spaces, deriving the parameter constraints in the different models. There is clearly no strong evidence for massive neutrinos, $w \neq -1$ or tensor modes, though they are certainly still compatible with the data in the ways we have explored.

One can make a more quantitative comparison of the different models by comparing how well each fits the data. As discussed in Appendix C a natural measure is the mean likelihood of the data obtained for the different models. Equivalently, if one chose a random sample from the possible parameter values, on average how well would it fit the data? Compared to the basic flat model with six varying parameters we find that the inflationary and general models both have a mean likelihood ratio close to 0.08. So by moving away from the basic model we have only decreased the average goodness of fit. Whilst certainly not ruled out, at the moment there is no evidence for observable effects from the more complicated models we have considered. Nonetheless, when considering parameter values, it is important to assess how dependent these are on the assumptions, and this can be seen by comparing the results we have presented. We conclude that at the moment simple inflationary models with small tilt and tensor amplitude (e.g. small field models with a nearly flat potential; or observationally equivalently, ekpyrotic models) account for the data well. There is no evidence for a cosmologically interesting neutrino mass, nor for the dark energy being anything other than a cosmological constant.

IV. CONCLUSIONS

In this paper we have demonstrated the power of Monte-Carlo techniques for determining cosmological constraints involving large numbers of parameters. Whilst our results using the current data are only of ephemeral interest, we have employed a general method that should be applicable into the future. Due to the enormously decreased number of likelihood evaluations in the MCMC method compared to other approaches, we are able to compute the theoretical predictions essentially exactly, and can account for the available data in detail. Once the chains have been computed importance sampling can be used to work out many further results, including taking account of new (consistent) data as it becomes available.

Our Monte-Carlo code and chains are publicly available at <http://cosmologist.info/cosmomc>.

Acknowledgments

We thank the members of the Leverhulme collaboration for many useful discussions, in particular Ofer Lahav, Carolina Ödman, Oystein Elgaroy and Jerry Ostriker. We are grateful to David MacKay and Steve Gull for encouraging the use of MCMC. We thank Anze Slozar, Keith Grainge and Alexandre Réfrégier for helpful suggestions. We thank George Efstathiou for making his CMBfit code available to us. AL thanks the Leverhulme Trust for support. SLB acknowledges support from Selwyn College and PPARC. We thank PPARC and HEFCE for support of the COSMOS facility.

APPENDIX A: THE METROPOLIS-HASTINGS ALGORITHM

The algorithm that we use for generating samples from the posterior distribution using a Markov Chain is called the Metropolis-Hastings algorithm. A Markov Chain moves from a position in parameter space θ_1 to next position θ_2 with transition probability $T(\theta_1, \theta_2)$, where θ labels a vector of parameter values. The Metropolis-Hastings transition kernel $T(\theta_1, \theta_2)$ is chosen so that the Markov Chain has a stationary asymptotic distribution equal to $P(\theta)$, where $P(\theta)$ is the distribution we wish to sample from. This is done by using an arbitrary *proposal density* distribution $q(\theta_n, \theta_{n+1})$ to propose a new point θ_{n+1} given the chain is currently at θ_n . The proposed new point is then accepted with probability

$$\alpha(\theta_n, \theta_{n+1}) = \min \left\{ 1, \frac{P(\theta_{n+1})q(\theta_{n+1}, \theta_n)}{P(\theta_n)q(\theta_n, \theta_{n+1})} \right\}$$

so that $T(\theta_n, \theta_{n+1}) = \alpha(\theta_n, \theta_{n+1})q(\theta_n, \theta_{n+1})$. This construction ensures that detailed balance holds,

$$P(\theta_{n+1})T(\theta_{n+1}, \theta_n) = P(\theta_n)T(\theta_n, \theta_{n+1}),$$

and hence that $P(\theta)$ is the equilibrium distribution of the chain.

If the chain is started in a random position in parameter space it will take a little time, *burn in*, to equilibrate before it starts sampling from the posterior distribution. After that time each chain position is a *correlated* sample from the posterior. The correlation is particularly obvious if the proposal is not accepted as then there are two or more samples at exactly the same point. However by sampling only occasional chain positions one can give the chain time to move to an uncorrelated position in parameter space, and one then obtains independent samples.

If the proposal density is symmetrical it cancels out when working out the acceptance probability, which then becomes just the ratio of the posteriors. This is the case when doing random walks where each successive position is a random perturbation from the previous one where the perturbation is independent of position. This is the case we consider.

The proposal density

The choice of the proposal density can have a large effect on how the algorithm performs in practice. In general one wants to have a proposal density that is the same shape as the posterior, ensuring that large changes are proposed to parameters along the degeneracy directions. Fortunately with cosmological data we have a good idea of what the posterior is likely to look like, and so choosing a sensible proposal density is not difficult.

If posteriors from models with common parameter are much easier to compute it can be very beneficial to use a proposal density that changes only a subset of the parameters on each iteration, ensuring that consecutive posterior evaluations only differ in a subset of the parameters. Proposing a change to a random subset of the parameters also increases the acceptance rate, especially in high dimensions, giving faster piecewise movement around parameter space. In the case of CMB parameter estimation models that differ only by a different normalization of the theoretical CMB power spectrum are very quick to compute from a single example. Similarly changing parameters that govern calibration uncertainties in the data can also be very quick. However changing parameters that govern the perturbation evolution, for example Ω_b , Ω_c , etc, will be much slower as in general it requires a detailed recalculation of the linear physics.

If we are comparing CMB data with theoretical models, the most general way to compute the theoretical C_l power spectrum is using a fast Boltzmann code such as CAMB [12] (a parallelized version of CMBFAST [13]; we discuss less accurate and general schemes below). Since the perturbation evolution is assumed to be linear, any parameters governing the initial power spectra of the scalar and tensor perturbations will be fast to compute once the transfer

function for each wavenumber has been computed. Parameters governing the initial power spectrum are therefore ‘fast’ parameters.

We therefore use a proposal density that makes changes only within the subsets of the fast and slow parameters, at least when we do not have an approximate covariance matrix available for the posterior.⁷. We have tried changing a random subset of one or two parameters at a time, and also cycling through the parameters in random order, which should give faster movement around parameter space. After one initial run one can use the covariance matrix to rotate to a more orthogonal parameter space before doing subsequent runs, allowing efficient exploitation of degeneracy information as long as the posterior is not highly non-Gaussian. Using CAMB running on a multi-processor machine, the computation of the CMB power spectra still dominates the time, but by changing ‘slow’ parameters only every few iterations rather than every iteration we save computation time, as well as getting better marginalization in the fast parameter directions.

The above scheme is sufficient for parameter estimation from current data, however as more data becomes available and the posterior becomes highly non-Gaussian or disjoint one may need to use more sophisticated schemes using simulated annealing, hybrid Monte Carlo, or schemes using cross-chain information [8, 9, 10].

APPENDIX B: IMPORTANCE SAMPLING

Given a set of samples from a distribution P , one can estimate quantities with respect to a different similar distribution P' , by weighting the samples in proportion to the probability ratios. This effectively gives a collection of non-integer weighted samples for computing Monte-Carlo estimates. For example the expected value of a function $f(\theta)$ under P' is given by

$$\begin{aligned} \langle f(\theta) \rangle_{P'} &= \int d\theta P'(\theta) f(\theta) = \int d\theta \frac{P'(\theta)}{P(\theta)} P(\theta) f(\theta) \\ &= \left\langle \frac{P'(\theta)}{P(\theta)} f(\theta) \right\rangle_P. \end{aligned} \quad (\text{B1})$$

Given a set $\{\theta_n\}$ of N samples from P one can therefore make the Monte-Carlo estimate

$$\langle f(\theta) \rangle_{P'} \approx \frac{1}{N} \sum_{n=1}^N \frac{P'(\theta_n)}{P(\theta_n)} f(\theta_n). \quad (\text{B2})$$

For this to work it is essential that P/P' is never very small, and for a good estimate without massively oversampling from P one needs $P'/P \sim \text{constant}$ everywhere where P' is significantly non-zero. If P' is non-zero over only a very small region compared to P it will be necessary to proportionately oversample from P .

If the distributions are not normalized, so that $\int d\theta P(\theta) = Z$, one can estimate the ratio of the normalizing constants using

$$\frac{Z'}{Z} = \left\langle \frac{P(\theta)'}{P(\theta)} \right\rangle_P \approx \frac{1}{N} \sum_{n=1}^N \frac{P'(\theta_n)}{P(\theta_n)},$$

and hence

$$\langle f(\theta) \rangle_{P'} \approx \frac{\sum_{n=1}^N P'(\theta_n)/P(\theta_n) f(\theta_n)}{\sum_{n=1}^N P'(\theta_n)/P(\theta_n)}. \quad (\text{B3})$$

In Bayesian analysis it can be useful to compute the ratio of the evidences $P(D) = \int d\theta P(D, \theta)$, given as above by

$$\frac{P'(D)}{P(D)} = \left\langle \frac{P'(\theta, D)}{P(\theta, D)} \right\rangle_{P(\theta|D)} \approx \frac{1}{N} \sum_{n=1}^N \frac{P'(D|\theta_n) P'(\theta_n)}{P(D|\theta_n) P(\theta_n)}, \quad (\text{B4})$$

⁷ When changing the slow parameters it is possible to also change the fast parameters at the same time. This can be a good idea when there are highly correlated slow and fast parameters, for example the reionization redshift and the tensor amplitude.

where the samples $\{\theta_n\}$ are drawn from $P(\theta|D)$. Assuming the distributions are sufficiently similar, the evidence under P' can therefore easily be computed from the probability ratios at a sample of points under P , and a known evidence under P . In many cases only the ratio is of interest — the ratio is larger than one if on average the probability of the samples under P' is higher than under P . In the case where the distributions are very different one may need to introduce a series of intermediate distributions that are all not too dissimilar to each other, and perform Monte Carlo simulations for each. The evidence ratio one requires is then just the product of that for all the intermediate distributions. Many more general schemes are described in [10, 37], though in this paper we only consider importance sampling to similar or subset distributions.

The simplest application of importance sampling is to adjust results for different priors. For example if one computes a chain with flat priors on the parameters, one may wish to importance sample to several different distributions with different priors on various parameters. This will work well as long as the prior does not skew the distribution too much or give non-zero weight to only a very small fraction of the models.

Faster Monte-Carlo

MCMC runs produce correlated samples from the probability distribution. To obtain independent samples one thins out the chain by a sufficiently large factor that the chain has had time to move to a randomly different point between the thinned samples. Depending on how one implements the MCMC, the shape of the posterior and the number of dimensions the thinning factor can be quite large, typically of the order ten to a thousand.

By performing Monte-Carlo simulations with a good approximation to the true probability distribution one can use importance sampling to correct the results with an accurate calculation of the probabilities. This can be useful if computing the probabilities accurately is much slower than computing an approximation, since one only ever importance samples *independent* samples. The burn-in and random walking stages of the Monte-Carlo involve a much larger number of probability evaluations, so by using a fast approximation when generating the chain one can save a lot of time.

Calculating the posterior from CMB data requires a calculation of the theoretical CMB power spectra, C_l . Using accurate codes like CAMB and CMBFAST is typically *much* slower than computing the likelihoods from the data once the C_l are known (assuming one uses a radical data-compression scheme, e.g. see Ref. [20]). In the not so distant future we will require to high accuracy C_l up to $l \sim 2500$, including second order effects such as lensing, and also also the the matter power spectrum at various redshifts. Unless one is fortunate enough to have access to a fast supercomputer this may be prohibitive.

With a small number of parameters it is possible to use a grid of models and interpolate to generate accurate C_l quickly, however as the number of parameters grows the computational cost of computing the grid grows exponentially. Also, as second order effects such as gravitational lensing become important, fast grid generation schemes such as the k -splitting scheme of Ref. [38] become much more difficult to implement accurately. However these may still be useful as fast approximation, as long as the independent samples are corrected with a more accurate calculation.

It is also possible to use fast semi-analytic schemes. Typically these are based on a smallish grid of base models, from which the C_l s in general models are computed quickly on the fly by accounting for changes in the angular diameter distance to last scattering, differing perturbation growth rates, etc. These approximate schemes can be made quite accurate at at small scales, with significant errors mainly at low l , precisely where the cosmic variance is large. So whilst an approximate scheme may produce small systematic errors in the likelihood, if the error is of the same order as the cosmic variance or less, the probabilities given the data are bound to be sufficiently similar for importance sampling to be valid.

A particular approximate C_l generator we have tried is CMBfit [39], which uses of combination of base C_l grids and analytic fits. This achieves quite good few percent level accuracy at high l , though larger systematic errors at low l . However the code is fast, and we found that importance sampling the results with an exact calculation of the C_l gives good results, and removes systematic biases introduced by the low l approximations. Such an approach can be generalized for more general late time evolution, for example models with quintessence where the effect on small scales is due almost entirely to changes in the background equation of state.

An alternative scheme based on grids of the transfer functions for each wavenumber can produce more accurate results, like the recently released DASH [40]. However this is not much faster than generating the C_l s exactly using CAMB on a fast multi-processor machine, and relies on a large pre-computed grid (which introduces its own limitations). The only real advantage over CMBfit is that more general initial power spectrum parameterization could be accounted for easily — something that is impossible with schemes based on grids of C_l s.

Even without a fast semi-analytic scheme, there are a variety of small corrections that can be applied post hoc. For example lensing effects the CMB C_l at the few percent level, so one may wish to compute chains without including

the lensing, then importance sample to correct the results using an accurate calculation including the lensing⁸. For small scales at high precision one may also wish to run CAMB at a high-accuracy setting to check that numerical errors in the default output are not affecting the results. Chains could be generated to lower l and the effect of the high- l constraints accounted for by importance sampling. For example we generated the chains using $l_{\max} = 1300$, and then for the independent samples re-computed the power spectra up to $l_{\max} = 2000$ for importance sampling with the CBI data.

Similar methods could be applied for the matter power spectrum using approximate fittings, see e.g. Refs. [38, 41]. However when a fast multi-processor machine is available, and one is interested in a very large number of parameters, it is a lot simpler to generate the entire chain using CAMB to generate the CMB power spectra and matter power spectrum, which is what we did for the results we present. The great advantage of this approach is that it generalises trivially if one wishes to include changes in the physics, for example different quintessence models, or changes in the initial power spectrum.

Constraints with new data

Assuming that one has some new data which is broadly consistent with the current data, in the sense that the posterior only shrinks, one can use importance sampling to quickly compute a new posterior including the new data. We have made our MCMC chains publicly available, so these can be used to rapidly compute new posteriors from new data without incurring any of the considerable computational cost of generating the original chain. For example if you believe in a tighter constraint on σ_8 than we have assumed, you just need to loop over the samples, adjusting the weights of the samples according to the ratio of the likelihood from the new constraint to likelihood from the broad constraint that we have assumed. Using importance sampling has the added benefit of making it very easy to assess how the new data is changing the posterior.

APPENDIX C: PARAMETER CONSTRAINTS

The great advantage of the Monte-Carlo approach is that you have a set of samples from the full parameter space. To answer any particular question one can examine the points and compute results reliably, taking full account of the shape of the posterior in N dimensions. However for human consumption it is usual to summarize the results as a set of parameter values and error bars, loosing most of the information about the shape of the distribution.

The simplest thing to do is to compute the marginalized 1-dimensional distributions for each parameter, essentially counting the number of samples within binned ranges of parameter values. Note that this is extremely hard to do using a brute-force numerical calculation as it scales exponentially with the number of dimensions, but is quite trivial from a set of Monte-Carlo samples. One can then quote the value at the maximum or mean of the 1D distribution, along with extremal values of the parameters which contain a fraction f of the samples, where f defines the confidence limit. The extremal values could be chosen so that there were the same number of outliers at both ends of the distribution, or such that the value of the *marginalized* probability is the same at each limit. This is a good way of summarizing the current state of knowledge as long as you have included everything you know, including using a believable prior over parameter space.

However frequently one wants to use the parameter estimates to assess consistency with new data or theories, and the prior can be very hard to define. For example, putting in a top hat prior on the age and H_0 , even if all of the other priors are flat broad top hats, the *marginalized* prior probabilities are *not* flat. This is because the marginalized distribution includes the effect of the amount of parameter space available at each point, which can depend quite strongly on the value of the parameter. Likewise it is possible to have a region in parameter space which fits the data rather well, but because the region is small the projected marginalized probability of those parameter values can be very low. Results from the marginalized distribution should therefore be interpreted with care.

When assessing consistency with new data (or theories), one really wants to know whether the posterior for the new data intersects the N -dimensional posterior for the current data in a region where both are likely. For example one could define the region of parameter space enclosing a fraction f of the points with the highest likelihood as one's N -dimensional confidence region, and then see whether this region intersects with the corresponding region for the new data. It is clearly sub-optimal to try to perform this comparison using only 1D parameter values and limits, however if one quotes the extremal values of each parameter contained in the N -dimensional confidence region it is

⁸ However if one is also computing the matter power spectrum numerically the additional cost of including the lensing effect is small.

at least possible to asses whether the N -dimensional regions might overlap. At least if the new data is outside these limits it is a clear indication that there is an inconsistency, whereas using the marginalized limits it shows no such thing (just that if there is a consistent region it makes up a small fraction of the original parameter space — something one would hope for if the new data is informative!) However it is of course easily possible for the 1D likelihood limits to be consistent but the full N -dimensional regions to be highly inconsistent.

Often it is useful to plot a curve showing the projected shape of the distribution in one dimension. One can plot the marginalized distribution, which shows fraction of the samples that occur per unit length in the one dimension. This can be misleading, as explained above, so it may also be a good idea to plot a curve of likelihood values. In Ref. [4] they plot the values of the likelihood of the best fit model at each value of the parameter, which shows useful complementary information. It is not so easy to compute this using a small set of Monte-Carlo samples however — mean values within each bin can be obtained quite accurately from a small number of samples, but getting a good value for the maximum in each bin requires a much larger number. It is also possible that the best-fit model at each value is finely tuned, and that most of the models at each value have much lower probability. As a compromise we plot the mean value of the likelihood of the samples in each bin. This is very easy to compute from the samples, and avoids the fine-tuning problem. It shows how good a fit you could expect if you drew a random sample from the marginalized distribution at each value of the parameter. Plots of both the maximum and the mean have the advantage of giving a flat curves for the prior if all the priors are top hats, unlike a plot of the marginalized distribution. Plotting the maximum however has an added advantage of avoiding the problem that priors are often parameterization dependent (e.g. constant in the parameter is not the same as constant in its log), making the marginalized and mean results dependent on parameterization of the other variables (unless one has a well justified prior, or uses a Jeffery's parameterization invariant prior, which is often not the case).

In order to be as informative as possible it can be useful to quote both the marginalized and likelihood limits, though of course one should study the full set of samples to make use of as much information as possible.

APPENDIX D: GOODNESS OF FIT

To consider whether an enlarged parameter space is justified, one ideally wants to compare the evidences $P(D)$ with the different parameter sets. In some cases, for example when using hyperparameter weights on experiments, it may be possible to define a prior on the extra parameters in which case one can compute the evidence ratio directly. The ratio does however depend quite strongly on the prior put on the parameters, which in general it is not straightforward to quantify. If one puts a broad prior on a parameter, but the likelihood is much narrower, the probability of the data is downweighted because the likelihood takes up a much smaller region of parameter space. One simple, but non-Bayesian, way to get round this is to set the prior equal to the normalized posterior for computing the evidence, in which case one compare the values of

$$'P(D)' = \frac{\int d\theta P(D|\theta)P(\theta|D)}{\int d\theta P(\theta|D)} \approx \frac{1}{N} \sum_{n=1}^N P(D|\theta_n).$$

This is just the expected probability of the data in the posterior distribution, which can be computed trivially from a set of Monte-Carlo samples as the mean likelihood of the samples. For Gaussian distributions this is the exponential mean of the chi-squareds under the posterior distribution, and is thus a smeared-out version of the common practice of quoting the chi-squared of the best fit. The smearing out helps to downweight extra parameters which have to be fine tuned to obtain better fits. If the mean likelihood is bigger with the extra parameters it suggests they are improving the fit to the data on average. Although we know no way to use the value rigorously for hypothesis testing, it seems nonetheless to be useful as a rule of thumb measure of goodness of fit.

APPENDIX E: CONSISTENCY OF DATA SETS

It is important to asses whether the datasets one is using are consistent, or whether one or more is likely to be erroneous. This can be done by introducing hyperparameter weights on the different datasets [42] when performing the analysis. If a dataset is inconsistent its posterior hyperparameter should have a low value, and the dataset then only contributes weakly to the posterior probability of the parameters. In the case that the likelihoods are of Gaussian form it is a simple matter to marginalize over the hyperparameters analytically given a simple prior. To assess whether the introduction of hyperparameters is justified (i.e. whether the data are inconsistent with respect to the model), one can compare the probability of getting the data in the two hypotheses: H_0 , no hyperparameters are needed; H_1 ,

hyperparameters are needed because one or more dataset is inconsistent. Using a maximum entropy prior assuming that on average the hyperparameter weights are unity, Ref. [42] gives

$$\frac{P(D|\theta, H_1)}{P(D|\theta, H_0)} = \prod_k \frac{2^{n_k/2+1}\Gamma(n_k/2+1)}{(\chi_k^2 + 2)e^{-\chi_k^2/2}},$$

where k labels the datasets, each of n_k points. Given a set of independent samples from H_0 it is straightforward to compute an estimate of the evidence ratio using Eq. (B4). If the datasets are inconsistent the importance sampling estimate would be very inaccurate as the probability distributions would be significantly different. However this should be clear when one computes the estimate since the probability ratios will vary wildly. If one suspects that one of the datasets is inconsistent it would probably be better to start with sampling from H_1 , and confirm that the evidence ratio supports using the hyperparameters.

An even simpler way of assessing consistency of the datasets is to assess the importance weights that one gets when adding or subtracting each dataset in turn from the likelihood calculation. Given a chain without a given dataset one can compute the mean likelihood of the samples. Then adding the dataset one does importance sampling to adjust the weights of the samples. Then using the weighted chain one can re-compute the mean likelihood without the given dataset. If this number is similar to the first number it indicates that the dataset is consistent with the others, in the sense that it is not significantly shifting the mean likelihood goodness of fit (Appendix D). Similarly one could simply assess whether then N -dimensional confidence interval without a given dataset intersects the confidence interval with the dataset.

APPENDIX F: ANALYTIC MARGINALIZATION

Frequently one has data in which there is an unknown calibration uncertainty, or an unknown normalization. These parameters can be marginalized over analytically following [21] as long as the likelihoods are Gaussian, and the priors on the amplitude parameter is Gaussian or flat. Typically one has a marginalization of the form

$$L \propto \int d\alpha P(\alpha) \exp[-(\alpha\mathbf{v} - \mathbf{d})^T \mathbf{N}^{-1}(\alpha\mathbf{v} - \mathbf{d})/2]$$

where \mathbf{v} and \mathbf{d} are vectors, \mathbf{N} is the noise covariance matrix, and $P(\alpha)$ is the prior. For example for the supernovae data \mathbf{v} is assumed to be a vector of equal constants giving the intrinsic magnitudes of the supernovae, and \mathbf{d} is a vector of the theoretical minus the observed effective magnitudes. If the prior $P(\alpha) = \text{const}$ it clearly cannot be normalized, however the marginalization is trivial giving

$$-2 \ln L = \mathbf{d}^T \left(\mathbf{N}^{-1} - \frac{\mathbf{N}^{-1} \mathbf{v} \mathbf{v}^T \mathbf{N}^{-1}}{\mathbf{v}^T \mathbf{N}^{-1} \mathbf{v}} \right) \mathbf{d} + \ln(\mathbf{v}^T \mathbf{N}^{-1} \mathbf{v}) + \text{const.}$$

In the case that \mathbf{v} is a constant (independent of the data and parameters), one has $L \propto e^{-\chi_{\text{eff}}^2/2}$ where

$$\chi_{\text{eff}}^2 = \mathbf{d}^T \left(\mathbf{N}^{-1} - \frac{\mathbf{N}^{-1} \mathbf{v} \mathbf{v}^T \mathbf{N}^{-1}}{\mathbf{v}^T \mathbf{N}^{-1} \mathbf{v}} \right) \mathbf{d} = \chi_{\text{best-fit}}^2.$$

This is exactly the same as the best-fit one obtains by minimising the likelihood w.r.t. α , and so in this case the maximization technique of Ref. [4] is exactly equivalent to full marginalization. For example, in the case of the supernovae data, marginalization with a flat prior over the magnitudes is equivalent to using the best-fit magnitude. In general this is not true as the logarithmic dependence $\ln(\mathbf{v}^T \mathbf{N}^{-1} \mathbf{v})$ can depend on the parameters. For example with the 2dF data \mathbf{v} would be the predicted matter power spectrum values, and α would be the unknown amplitude relative to the galaxy power spectrum at $z = 0.17$.

[1] L. et al. (2002), astro-ph/0112162.
[2] E. et al. (2002), astro-ph/0109152.
[3] L. Knox, N. Christensen, and C. Skordis, *Astrophys. J.* **563**, L95 (2001), URL http://adsabs.harvard.edu/cgi-bin/nph-bib_query?bibcode=2001ApJ...563L..95K&db_key=AST.
[4] X. Wang, M. Tegmark, and M. Zaldarriaga (2002), *phys. Rev. D* (to be published), astro-ph/0105091.

- [5] C.B. Netterfield et al. (2001), astro-ph/0104460.
- [6] P. de Bernardis, P. Ade, J. Bock, J. Bond, J. Borrill, A. Boscaleri, K. Coble, C. Contaldi, B. Crill, G. D. Troia, et al. (2001), astro-ph/0105296.
- [7] C. Pryke, N. W. Halverson, E. M. Leitch, J. Kovac, J. E. Carlstrom, W. L. Holzapfel, and M. Dragovan, *Astrophys. J.* **568**, 46 (2002), URL http://adsabs.harvard.edu/cgi-bin/nph-bib_query?bibcode=2002A&J...568...46P&db_key=AST.
- [8] D. Gamerman, *Markov Chain Monte Carlo: Stochastic simulation for Bayesian inference* (Chapman and Hall, 1997).
- [9] D. J. C. MacKay (2002), <http://www.inference.phy.cam.ac.uk/mackay/itprnn/book.html>.
- [10] R. M. Neil (1993), <ftp://ftp.cs.utoronto.ca/pub/~radford/review.ps.Z>.
- [11] N. Christensen, R. Meyer, L. Knox, and B. Luey, *Class. Quant. Grav.* **18**, 2677 (2001), astro-ph/0103134.
- [12] A. Lewis, A. Challinor, and A. Lasenby, *Astrophys. J.* **538**, 473 (2000), astro-ph/9911177.
- [13] U. Seljak and M. Zaldarriaga, *Astrophys. J.* **469**, 437 (1996), astro-ph/9603033.
- [14] C. L. Bennett, et al., *Astrophys. J. Lett.* **464** (1996).
- [15] S. Hanany et al., *Astrophys. J.* **545**, L5 (2000), astro-ph/0005123.
- [16] N. W. Halverson et al. (2001), astro-ph/0104489.
- [17] P. F. Scott et al. (2002), astro-ph/0205380.
- [18] T. J. Pearson et al. (2002), astro-ph/0205388.
- [19] J. R. Bond et al. (2002), astro-ph/0205386.
- [20] J. R. Bond, A. H. Jaffe, and L. E. Knox, *Astrophys. J.* **533**, 19 (2000), astro-ph/9808264.
- [21] S. L. Bridle, R. Crittenden, A. Melchiorri, M. P. Hobson, R. Kneissl, and A. N. Lasenby (2001), astro-ph/0112114.
- [22] R. A. Rubiño-Martin et al. (2002), astro-ph/0205367.
- [23] t. . W. L. Freedman et al. (????).
- [24] S. Seager, D. Sasselov, and D. Scott (1999), astro-ph/9909275.
- [25] S. Burles, K. M. Nollett, and M. S. Turner, *Astrophys. J.* **552**, L1 (2001), astro-ph/0010171.
- [26] S. Perlmutter, G. Aldering, G. Goldhaber, R. A. Knop, P. Nugent, P. G. Castro, S. Deustua, S. Fabbro, A. Goobar, D. E. Groom, et al., *Astrophys. J.* **517**, 565 (1999), astro-ph/9812133.
- [27] A. Cooray (2002), astro-ph/0203048.
- [28] K. Subramanian and J. D. Barrow (2002), astro-ph/0205312.
- [29] M. Tegmark, A. Hamilton, and Y. Xu (2002), astro-ph/0111575.
- [30] T. Toshito et al. (Super-Kamiokande collaboration) (2001), hep-ex/0105023.
- [31] V. Barger, S. L. Glashow, D. Marfatia, and K. Whisnant (2002), *phys. Lett. B* (to be published), hep-ph/0201262.
- [32] A. Lewis and A. Challinor (2002), astro-ph/0203507.
- [33] S. M. Leach, A. R. Liddle, J. Martin, and D. J. Schwarz (2002), astro-ph/0202094.
- [34] O. Elgaroy et al. (2002), astro-ph/0204152.
- [35] S. Hannestad (2002), astro-ph/0205223.
- [36] S. Gratton, A. Lewis, and N. Turok, *Phys. Rev. D* **65**, 043513 (2002), astro-ph/0111012.
- [37] R. M. Neil, *Statistics and Computing* **11**, 125 (2001), <http://www.cs.toronto.edu/~radford/ais-pub.abstract.html>.
- [38] M. Tegmark, M. Zaldarriaga, and A. J. S. Hamilton, *Phys. Rev. D* **63**, 043007 (2001), astro-ph/0008167.
- [39] G. Efstathiou et al (2001), astro-ph/0109152.
- [40] M. Kaplinghat, L. Knox, and C. Skordis (2002), astro-ph/0203413.
- [41] D. J. Eisenstein and W. Hu, *Astrophys. J.* **511**, 5 (1999), astro-ph/9710252.
- [42] M. P. Hobson, S. L. Bridle, and O. Lahav (2002), astro-ph/0203259.